# Roundness Errors in BTA Drilling and a Model of Waviness and Lobing Caused by Resonant Forced Vibrations of Its Long Drill Shaft

**Chyn-Shu Deng**
Department of Mechanical Engineering,
National Lien-Ho University,
Miaoli, Taiwan, Republic of China

**Jih-Hua Chin**
Mem.ASME;
e-mail: jhchin@mail.nctu.edu.tw
Department of Mechanical Engineering,
National Chiao Tung University,
Hsinchu, Taiwan, Republic of China

*The original purpose of this work was to propose an equation system to describe the kind of drilling in which the tools are with pronounced shaft length. The equation system turned out to disclose the low frequency mechanism of hole lobes. The proposed system is composed of Euler-Bernoulli beam equation representing tool shaft, and an excitation force in form of Fourier series. An empirical cutting force was established and related cutting force components were calculated. And the accumulated contribution of modes and harmonics was evaluated. The solution for the proposed equation system allowed a prediction of hole roundness which was consistent with experimental results for different conditions. The solution also allowed an investigation into the waviness and lobes. The results suggested that the bizarre phenomenon of lobes on hole is in reality waviness described by Tlusty for milling. The rigorous mathematical nature of the proposed equation built solid foundation for former empirical observation of waviness and lobes on work pieces.* [DOI: 10.1115/1.1765142]

## 1 Introduction

Deep-hole drilling is one of the most important processes for the production of a high-precision workpiece with high-quality holes. Its main areas of application are in the defense, aircraft and automobile industries. Since the ratio of hole-depth to hole-diameter exceeds ten, a long tool shaft is needed which claims its own dynamics when machining. This is also true in milling with long shaft milling tools. The dynamic cutting force excites the long shaft, inducing a vibration/deflection which causes inaccuracy such as hole tolerances, roundness error and even a system problem known as chatter vibration.

The machining quality of deep-hole drilling has been studied for various machining conditions [1–5]. Sakuma et al. [6] carried out experimental work and proposed simple formulas for the burnishing action of guide pads. They also discussed the influence of various machining conditions on the hole accuracies for a BTA (boring and trepanning association) drilling process. Sakuma et al. [7,8] considered the behavior of the BTA solid boring system as that of a four-edge cutting tool and postulated that the forming of a multi-corner hole is a certain kind of self-excited vibration.

Gessesse et al. [9] investigated the formation of spiraling or helical multi-lobe holes produced by BTA machining. Chin and Lin [10] discussed the stability of the drilling process by treating the tool shaft as a second order lumped mass system. Chandrashekhar et al. [11] proposed a three-dimensional model of the BTA machining system including the interaction between the stationary workpiece and the rotating tool. Chandrashekhar et al. [12] used the helical grooves to predict the roundness error of the drilled workpiece, but there were obvious discrepancies between theoretical and experimental results. Chin et al. [13,14] proposed a mathematical model to simulate chip flowing in Gundrill and monitored the pressure of the chip-carrying fluid by using a piezoelectric transducer. Deng et al. [15] used beam theory to investigate the hole straightness as affected by pilot bushing and intermediate support misalignments.

Literature investigation reveals that there are no rigorous theories to study the effect of the dynamic cutting force on machining hole quality especially when there is a participation of shaft dynamics. The purpose of this study is to propose governing equations for the drilling process, the solution of which is able to give answers to phenomena observed by empirical studies. The system governing equations proposed were composed of the Euler-Bernoulli beam equation [16–18] and an excitation force expressed in Fourier series. Solutions were found by introducing empirically calibrated excitation forces, and a comparison between solutions and experimental results was made. Finally, the low-frequency mechanism of lobe formation was discussed and it was shown that the lobes in deep-hole drilling were in reality a phenomenon of waviness described by Tlusty [19] for high-speed milling. Lobes mechanisms in reaming and twist drilling were also cross-referenced [20–23]. The proposed system equations provided a solid theoretical ground for machining in which the tools have pronounced shaft dynamics.

## 2 System Construction

**2.1 The Construction of Excitation Force.** Figure 1 shows the drill head of a BTA drilling tool [24]. The cutting force system comprises forces from the cutting edge at point A and two burnishing pads at points B and C. The cutting force system is balanced in radial direction, so the radial excitation force $f(t)$ on tool can be expressed as:

$$f(t)=f_A+f_B+f_C \tag{1}$$

Traditionally, the cutting force was determined in relation to the area of the uncut chip, or to the cutting depth if the cutting width was kept constant. This nonlinear force mechanism brings hardly any physical insight into the system when used directly as the excitation force on the tool shaft. Here a departure from the real cutting force mechanism is chosen, in which the force is decom-

Contributed by the Manufacturing Engineering Division for publication in the JOURNAL OF MANUFACTURING SCIENCE AND ENGINEERING. Manuscript received June 2003; Revised Jan. 2004. Associate Editor: Y. C. Shin.

  

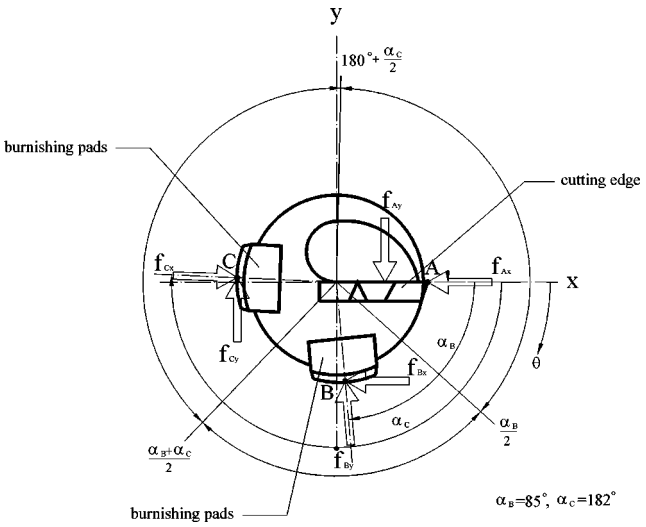


**Fig. 1 Cutting force system of BTA drilling [24]**

posed into harmonic components. Matin and Rahman [25] were the first to treat the force as a Fourier series. Based on a similar idea, the cutting force on the cutting edge and the burnishing pads in the longitudinal direction (z axis) can be represented by harmonic functions as follows:

$$f_A=\frac{a_{0A}}{2}+\sum_{m=1}^{\infty}\{[a_{mA}\cos(m\theta)+b_{mA}\sin(m\theta)]e^{jm\omega(t-z/c_w)}\} \tag{2}$$

$$f_B=\frac{a_{0B}}{2}+\sum_{m=1}^{\infty}\{[a_{mB}\cos m(\theta+\alpha_B)+b_{mB}\sin m(\theta+\alpha_B)]e^{jm\omega(t-z/c_w)}\} \tag{3}$$

$$f_C=\frac{a_{0C}}{2}+\sum_{m=1}^{\infty}\{[a_{mC}\cos m(\theta+\alpha_C)+b_{mC}\sin m(\theta+\alpha_C)]e^{jm\omega(t-z/c_w)}\} \tag{4}$$

where $m$ is the harmonic number, $a_{0A}$, $a_{0B}$, $a_{0C}$, $a_{mA}$, $a_{mB}$, $a_{mC}$, $b_{mA}$, $b_{mB}$ and $b_{mC}$ are Fourier coefficients, $j=\sqrt{-1}=\pi/2$ (in polar form), $t$ is time, $\omega$ is the angular speed of the tool, $c_w$ is the wave speed in the workpiece and $c_w=\sqrt{E/\rho}$ [26].

Based on Eqs. (2)–(4), the forces $f_{Ax}$, $f_{Ay}$, $f_{Bx}$, $f_{By}$, $f_{Cx}$ and $f_{Cy}$ can be expressed by harmonic functions as follows:

$$f_{Ax}=\frac{a_{0A}}{2}+\sum_{m=1}^{\infty}[a_{mA}\cos(m\theta)e^{jm\omega(t-z/c_w)}] \tag{5}$$

$$f_{Ay}=\sum_{m=1}^{\infty}[b_{mA}\sin(m\theta)e^{jm\omega(t-z/c_w)}] \tag{6}$$

$$f_{Bx}=\frac{a_{0B}}{2}+\sum_{m=1}^{\infty}[a_{mB}\cos m(\theta+\alpha_B)e^{jm\omega(t-z/c_w)}] \tag{7}$$

$$f_{By}=\sum_{m=1}^{\infty}[b_{mB}\sin m(\theta+\alpha_B)e^{jm\omega(t-z/c_w)}] \tag{8}$$

$$f_{Cx}=\frac{a_{0C}}{2}+\sum_{m=1}^{\infty}[a_{mC}\cos m(\theta+\alpha_C)e^{jm\omega(t-z/c_w)}] \tag{9}$$

$$f_{Cy}=\sum_{m=1}^{\infty}[b_{mC}\sin m(\theta+\alpha_C)e^{jm\omega(t-z/c_w)}] \tag{10}$$

Integrating Eqs. (5)–(10) at the mid position between any two cutting edges, the Fourier coefficients $a_{mA}$, $a_{mB}$, $a_{mC}$, $b_{mA}$, $b_{mB}$ and $b_{mC}$ are determined:

$$a_{mA}=\frac{1}{\pi}\int_{-(360°-\alpha_C/2)}^{\alpha_B/2}f_{Ax}\cos(m\theta)d\theta=\frac{f_{Ax}}{m\pi}\left[\sin m\left(\frac{\alpha_B}{2}\right)+\sin m\left(\frac{360°-\alpha_C}{2}\right)\right] \tag{11}$$

$$b_{mA}=\frac{1}{\pi}\int_{-(360°-\alpha_C/2)}^{\alpha_B/2}f_{Ay}\sin(m\theta)d\theta=\frac{f_{Ay}}{m\pi}\left[\cos m\left(\frac{360°-\alpha_C}{2}\right)-\cos m\left(\frac{\alpha_B}{2}\right)\right] \tag{12}$$

$$a_{mB}=\frac{1}{\pi}\int_{\alpha_B/2}^{\alpha_B+\alpha_C/2}f_{Bx}\cos m(\theta+\alpha_B)d\theta=\frac{f_{Bx}}{m\pi}\left[\sin m\left(\frac{3\alpha_B+\alpha_C}{2}\right)-\sin m\left(\frac{3\alpha_B}{2}\right)\right] \tag{13}$$

$$b_{mB}=\frac{1}{\pi}\int_{\alpha_B/2}^{\alpha_B+\alpha_C/2}f_{By}\sin m(\theta+\alpha_B)d\theta=\frac{f_{By}}{m\pi}\left[\cos m\left(\frac{3\alpha_B}{2}\right)-\cos m\left(\frac{3\alpha_B+\alpha_C}{2}\right)\right] \tag{14}$$

$$a_{mC}=\frac{1}{\pi}\int_{\alpha_B+\alpha_C/2}^{360°+\alpha_C/2}f_{Cx}\cos m(\theta+\alpha_C)d\theta=\frac{f_{Cx}}{m\pi}\left[\sin m\left(\frac{360°+3\alpha_C}{2}\right)-\sin m\left(\frac{\alpha_B+3\alpha_C}{2}\right)\right] \tag{15}$$

$$b_{mC}=\frac{1}{\pi}\int_{\alpha_B+\alpha_C/2}^{360°+\alpha_C/2}f_{Cy}\sin m(\theta+\alpha_C)d\theta=\frac{f_{Cy}}{m\pi}\left[\cos m\left(\frac{\alpha_B+3\alpha_C}{2}\right)-\cos m\left(\frac{360°+3\alpha_C}{2}\right)\right] \tag{16}$$

The constant terms of Eqs. (5), (7), and (9) can be obtained by setting $m=0$ in Eqs. (11), (13) and (15) which yield:

$$\frac{a_{0A}}{2}=\frac{f_{Ax}}{2\pi}\left(\pi+\frac{\alpha_B-\alpha_C}{2}\right) \tag{17}$$

$$\frac{a_{0B}}{2}=\frac{f_{Bx}}{2\pi}\left(\frac{\alpha_C}{2}\right) \tag{18}$$

$$\frac{a_{0C}}{2}=\frac{f_{Cx}}{2\pi}\left(\pi-\frac{\alpha_B}{2}\right) \tag{19}$$

Equations (1) and (2)–(4) describe the excitation force $f(z,t)$ in harmonic form.

Therefore, the radial excitation force is constructed as

$$f(z,t)=\frac{a_{0A}+a_{0B}+a_{0C}}{2}+\sum_{m=1}^{\infty}\{[a_{mA}\cos m(\omega t)+b_{mA}\sin m(\omega t)+a_{mB}\cos m(\omega t+\alpha_B)+b_{mB}\sin m(\omega t+\alpha_B)+a_{mC}\cos m(\omega t+\alpha_C)+b_{mC}\sin m(\omega t+\alpha_C)]e^{jm\omega(t-z/c_w)}\} \tag{20}$$

where the Fourier coefficients $a_{0A}$, $a_{0B}$, $a_{0C}$, $a_{mA}$, $a_{mB}$, $a_{mC}$, $b_{mA}$, $b_{mB}$ and $b_{mC}$ are determined by Eqs. (11)–(19).

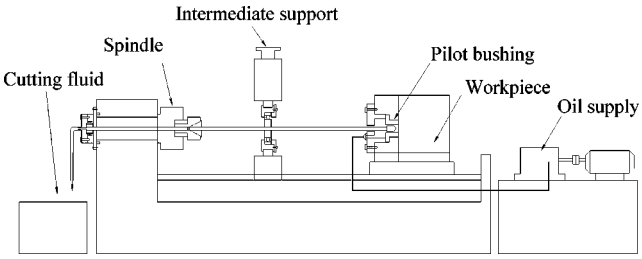


**Fig. 2 BTA drilling stystem**

**2.2 The Governing Equation for the Tool Shaft.** The tool shaft was studied by using the Euler-Bernoulli model. Based on Perng and Chin [18], the governing equation for the tool shaft is as follows:

$$EI\frac{\partial^4(\Delta R)}{\partial z^4}+\rho A\frac{\partial^2(\Delta R)}{\partial t^2}+j2\omega\rho A\frac{\partial(\Delta R)}{\partial t}-\omega^2\rho A(\Delta R)=0$$
$$\Delta R=\sqrt{(\Delta x)^2+(\Delta y)^2} \tag{21}$$

The boundary condition of clamping side (spindle side in Fig. 2) of shaft was assumed to be fixed and that of the cutting and burnishing side was assumed to be simply supported [15].

**2.3 The Dynamic Radial Deflection.** Equation (21) creates a homogenous solution, which is the transient state response of tool shaft dissipating with time. Its non-homogenous solution, which represents the steady state response, is responsible for describing the drilling process. Therefore, the following system equation shall govern the kind of drilling process in which tool shaft takes an essential part.

$$EI\frac{\partial^4(\Delta R)}{\partial z^4}+\rho A\frac{\partial^2(\Delta R)}{\partial t^2}+j2\omega\rho A\frac{\partial(\Delta R)}{\partial t}-\omega^2\rho A(\Delta R)$$
$$=f(z,t)\,\delta(z-\ell) \tag{22}$$

The physical meaning of the left-hand side terms are:

$$EI\frac{\partial^4(\Delta R)}{\partial z^4}:\ \text{restoring force}\qquad \rho A\frac{\partial^2(\Delta R)}{\partial t^2}:\ \text{inertia force;}$$

$$j2\omega\rho A\frac{\partial(\Delta R)}{\partial t}:\ \text{damping force}$$

$$\omega^2\rho A(\Delta R):\ \text{centrifugal force.}$$

In order to make the units of both sides consistent, the terms in the right side of Eq. (22) are multiplied by a Dirac-delta function, defined as [27]:

$$\delta(z-\ell)=\begin{cases}\infty & z=l\\ 0 & \text{otherwise}\end{cases} \tag{23}$$

Equation (22) governs the radial (lateral) motion of the tool shaft when excited by the radial excitation force modeled in Eq. (20). The solution of Eq. (22) determines the shape or distortion of the machined hole, which can be found by letting

$$\Delta R(z,t)=\sum\ \phi(z)q(t) \tag{24}$$

where $\phi(z)$ is a shape function obtained from the homogenous equation and expressed by

$$\phi_n(z)=c_1\cosh(k_nz)+c_2\sinh(k_nz)+c_3\cos(k_nz)+c_4\sin(k_nz) \tag{25}$$

**Table 1 The value of $k_n\ell$ of *n*th mode**

| | $n=1$ | $n=2$ | $n=3$ | $n=4$ | $n=5$ |
|---|---|---|---|---|---|
| $k_n\ell$ | 3.9266 | 7.0686 | 10.2102 | 13.3518 | 16.4934 |

where the subscript "$n$" is the mode number, $c_1$, $c_2$, $c_3$, and $c_4$ are constants, $k_n$ is an undetermined constant of the $n$th mode. For a fixed, simply supported beam, the beam characteristic is expressed as [30]

$$\tan(k_n\ell)-\tanh(k_n\ell)=0 \tag{26}$$

where $k_n\ell$ can be obtained by solving Eq. (26), and its values for mode $n=1\sim5$ are listed in Table 1.

Substituting Eq. (25) into Eq. (24) gives

$$\Delta R(z,t)=\sum_{n=1}^{\infty}\{q_1(t)\cosh(k_nz)+q_2(t)\sinh(k_nz)+q_3(t)\cos(k_nz)$$
$$+q_4(t)\sin(k_nz)\} \tag{27}$$

where $q_1(t)$, $q_2(t)$, $q_3(t)$, and $q_4(t)$ are time variables.

The dynamic radial deflection can be obtained from (27):

$$\Delta R(z,t)=\sum_{n=1}^{\infty}\left\{2k_n\left[\frac{q_6(t)\cosh(k_n\ell)\cosh(k_nz)}{2k_n\ell+\sinh(2k_n\ell)}\right.\right.$$
$$+\frac{q_7(t)\sinh(k_n\ell)\sinh(k_nz)}{\sinh(2k_n\ell)-2k_n\ell}+\frac{q_6(t)\cos(k_n\ell)\cos(k_nz)}{2k_n\ell+\sin(2k_n\ell)}$$
$$\left.\left.+\frac{q_7(t)\sin(k_n\ell)\sin(k_nz)}{2k_n\ell-\sin(2k_n\ell)}\right]\right\} \tag{28}$$

where $k_n\ell$ is shown in Table 1, $q_6(t)$ and $q_7(t)$ are listed in Appendix A.

Equation (28) allows a precise determination of dynamic radial deflection contributed by tool shaft vibration.

**2.4 The Roundness Error for the Hole Profile.** The hole roundness error is an index for hole quality, which can be examined only by experiments in the past. Since Eq. (28) describes the dynamic radial deflection in response to the excitation force, it shall be able to predict the roundness of hole for different machining conditions.

A hole profile with roundness error is shown in Fig. 3 [28] in which the roundness error is defined as follows:

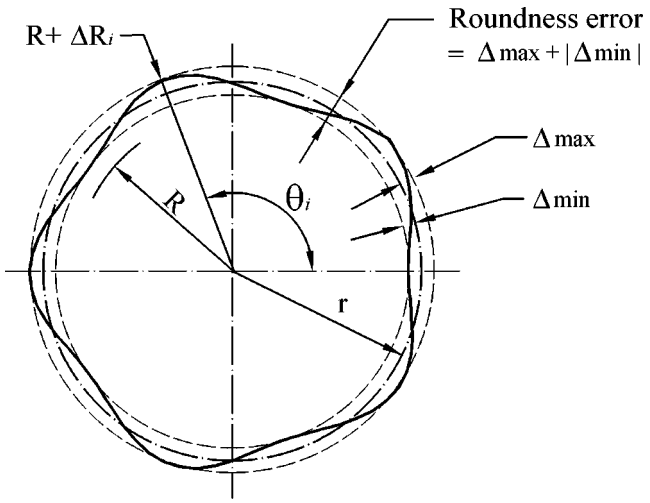


**Fig. 3 Hole profile [28]**

**Table 2 Machining conditions**

| Feed rate (mm/rev) | Tool diameter (mm) | Rotational speed (rpm) | Shaft length (mm) |
|---|---|---|---|
| 0.05 | 18.91 | 215 | 1200 |
| 0.07 | 19.90 | 390 | 1600 |
| 0.10 | 24.11 | 585 | |
| | 26.40 | 855 | |

$$\text{Roundness error} = \Delta_{\max} + |\Delta_{\min}| \tag{29}$$

$$\Delta_i = (R + \Delta R_i) - r - a\cos\theta_i - b\sin\theta_i$$

$$r = \frac{1}{k}\sum_{i=1}^{k}(R + \Delta R_i)$$

$$a = \frac{2}{k}\sum_{i=1}^{k}(R + \Delta R_i)\cos\theta_i \tag{30}$$

$$b = \frac{2}{k}\sum_{i=1}^{k}(R + \Delta R_i)\sin\theta_i$$

$\Delta R_i$: dynamic radial deflection at tool rotation angle $\theta_i$.

$r$: the radius of the least square circle (LSC).

$\Delta_{\max}$: the maximum distance between the outer radius and the radius of the least square circle (the maximum of $\Delta_i$).

$\Delta_{\min}$: the minimum distance between the inner radius and the radius of the least square circle (the minimum of $\Delta_i$).

$\Delta_i$: profile deviation with reference to least square circle at $\theta_i$.

$k$: number of the equi-spaced points on hole profile.

Theoretical prediction of roundness error can be made by obtaining dynamic radial deflection $\Delta R_i$ from Eq. (28) and calculating Eqs. (29) and (30).

## 3 Experiments

The purpose of experiments is to compare the theoretical and experimental roundness errors obtained under different drilling conditions as listed in Table 2. The experiments were performed on a retrofitted machine (Fig. 2 and Appendix B), which can accommodate BTA deep-hole drilling to examine the dynamic effects of the long tool shaft on hole distortion.

The workpiece material was AISI 1045 steel sized $\phi 50\times 300$ mm, which was drilled to a depth of 280 mm and subsequently cut into ten equal pieces (25 mm length). The roundness errors were measured along the length of drilled hole using a Mitutoyo (RA-2 type), which utilizes the least square circle method (LSC) to express a hole profile.

Experimental forces were also measured, for which the setup is shown in Fig. 4. The forces sampled by data acquisition system (microlink) were processed to establish an empirical model of primary tangential force $f_{Ay}$ using MATHEMATICAS software. This empirical force model was used in the proposed governing equation.

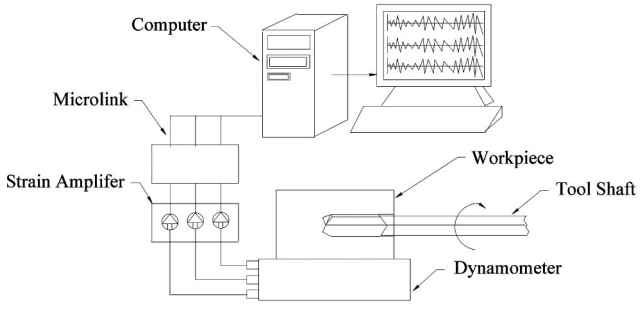


**Fig. 4 Experimental setup for measuring cutting force**

## 4 Results and Discussion

**4.1 Empirical Model for Primary Tangential Forces $f_{Ay}$.** Although the dominant part of forces takes place on the cutting edge, burnishing forces on the pads (B, C in Fig. 1) also contribute to the force system. Let $f_{tx}$ and $f_{ty}$ be forces in x- and y-direction in Fig. 1, the following balances hold:

$$f_{tx} = -f_{Ax} - f_{Bx}\cos\beta - f_{By}\sin\beta + f_{Cx}\cos\gamma + f_{Cy}\sin\gamma \tag{31}$$

$$f_{ty} = -f_{Ay} - f_{Bx}\sin\beta + f_{By}\cos\beta - f_{Cx}\sin\gamma + f_{Cy}\cos\gamma$$

$$\beta = 90° - \alpha_B \tag{32}$$

$$\gamma = \alpha_C - 180°$$

Among these forces $f_{Ax}$, $f_{Ay}$ is the primary radial and tangential force on the cutting edge, while $f_{Bx}$, $f_{By}$, $f_{Cx}$, $f_{Cy}$ are forces on burnishing pads.

It is generally true that the radial force and tangential force stand in a constant relationship. Griffiths [24] reported that the ratios of the primary tangential force $f_{Ay}$ to the forces $f_{Bx}$, $f_{By}$, $f_{Cx}$ and $f_{Cy}$ were as follows:

$$\begin{array}{cccccc} f_{Ay}: & & f_{Bx} & f_{By} & f_{Cx} & f_{Cy} \\ 1: & & 0.16 & 0.94 & 0.54 & 0.09 \end{array} \tag{33}$$

Besides, the relationships between the primary radial force, $f_{Ax}$, and the primary tangential force, $f_{Ay}$, were further reported by Griffiths [24] as

$$f_{Ax} = 0.19 f_{Ay} \quad \text{at feed rate } 0.05 \text{ mm/rev}, \tag{34}$$

$$f_{Ax} = 0.23 f_{Ay} \quad \text{at feed rate } 0.07 \text{ mm/rev}, \tag{35}$$

$$f_{Ax} = 0.29 f_{Ay} \quad \text{at feed rate } 0.10 \text{ mm/rev}, \tag{36}$$

While the exact proportions between the involved forces may vary in different cases, they offer common advantage that not all the forces are independent unknowns. Making use of empirical root-mean-square data and the relationships Eqs. (33)–(36), the primary tangential force $f_{Ay}$ can be formulated by using MATHEMATICAS as

$$f_{Ay} = 1.502 d^{-0.11} s^{2.01} N^{2.00} \ell^{0.02} z^{-0.09} \tag{37}$$

Other force components $f_{Ax}$, $f_{Bx}$, $f_{By}$, $f_{Cx}$, and $f_{Cy}$ stand in empirical relationships with $f_{Ay}$, hence the entire force system can be established. With these forces the Fourier coefficients $a_{0A}$, $a_{0B}$, $a_{0C}$, $a_{mA}$, $a_{mB}$, $a_{mC}$, $b_{mA}$, $b_{mB}$ and $b_{mC}$ in Eqs. (11)–(19) and the excitation force $f(z,t)$ of Eq. (20) can be determined.

**4.2 The Contribution of Number of Modes and Harmonics.** The shaft of BTA tool is a kind of solid continuum beam. The solution of its governing equation contains infinite numbers of harmonics and modes. Equation (28) allows an investigation into the accumulated contribution of harmonics and mode numbers to the dynamic radial deflection. Figure 5 showed such contributions. It is seen that the major dynamic radial deflection is contributed by the first mode ($n=1$) and the first harmonic ($m=1$).

The numbers of modes appeared in the tool vibration do not make significant difference in creation of the radial deflection. And the numbers of harmonics make slight difference but beyond $m=14$ the difference becomes insignificant. The error percentage of dynamic radial deflection is less than 0.1% for $m=1\sim 24$ and $m=1\sim 25$, or for $n=1\sim 4$ and $n=1\sim 5$. For cautious sake, in the following simulation $m=1\sim 24$ and $n=1\sim 4$ were used in Eq. (28).

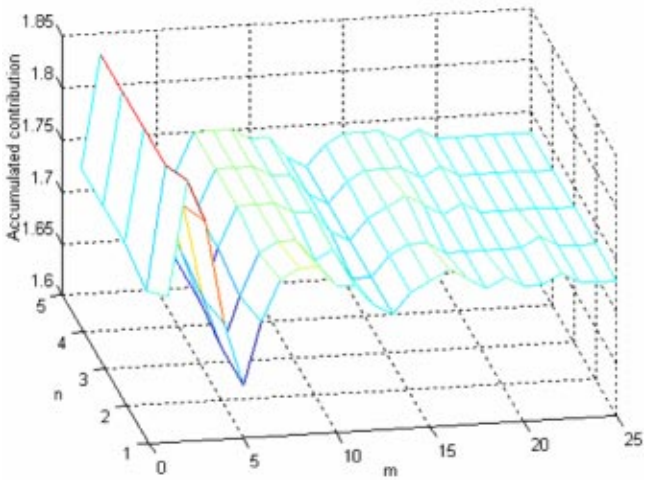


**Fig. 5 Accumulated contribution of number of modes (n) and number of harmonics (m) to the dynamic radial deflection ($\mu$m). Tool diameter: 18.91 mm; feed rate: 0.05 mm/rev; tool speed: 585 rpm; shaft length: 1600 mm; hole depth: 250 mm.**

**4.3 The Analysis of the Hole Roundness Error.** Figure 6 shows a sample of the hole roundness error recorded by Mitutoyo. The comparisons of values predicted by Eq. (28) with experimental results are shown in Figs. 7–9. Figure 7 shows the influence of feed rates on the hole roundness error. It is seen that the higher the feed rate, the greater the roundness error. This is because at higher feed rate the chip load becomes larger and the tool bears greater cutting force. The trend conforms to the results reported by Chandrashekhar et al. [29]. Moreover, the roundness errors at entry are higher but decrease with penetration depth. These may be due to the unstable beginning of drilling process. Figure 8 shows the influence of tool speeds on the hole roundness error. It reveals that the higher the rotational speeds the bigger the roundness error. The reason for this is the shaft vibration and whips at higher speeds [1]. Figure 9 shows the influence of shaft lengths and tool diameters on the hole roundness error. It is shown that longer shafts and smaller tool diameters yield bigger roundness error. This is because that longer shaft is less stiff, which leads to bigger deflection. And the tool with smaller diameter is less rigid than the tool with larger diameter.

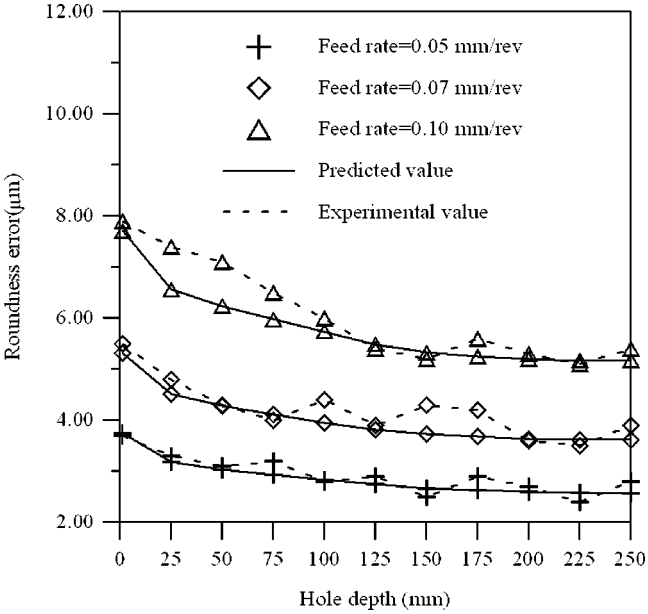


**Fig. 7 Influence of feed rates on the hole roundness error, tool diameter: 18.91 mm; rotational speed: 585 rpm; shaft length: 1600 mm**

Figures 7–9 show that the experimental and theoretical values of the roundness error are in agreement in both trend and magnitude. The error percentage between both was less than 10%. This discrepancy is reasonable since the tool shaft was clamped by jaws, which is less ideal than the ''built-in'' boundary conditions used in the equations.

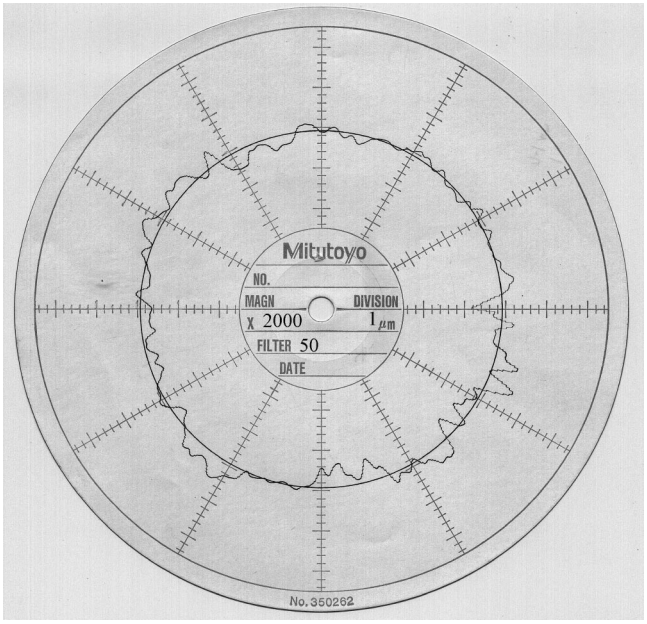


**Fig. 6 Hole roundness error: 7.1 $\mu$m; tool diameter: 18.91 mm; rotational speed: 585 rpm; shaft length: 1600 mm; feed rate: 0.1 mm; hole depth: 50 mm**

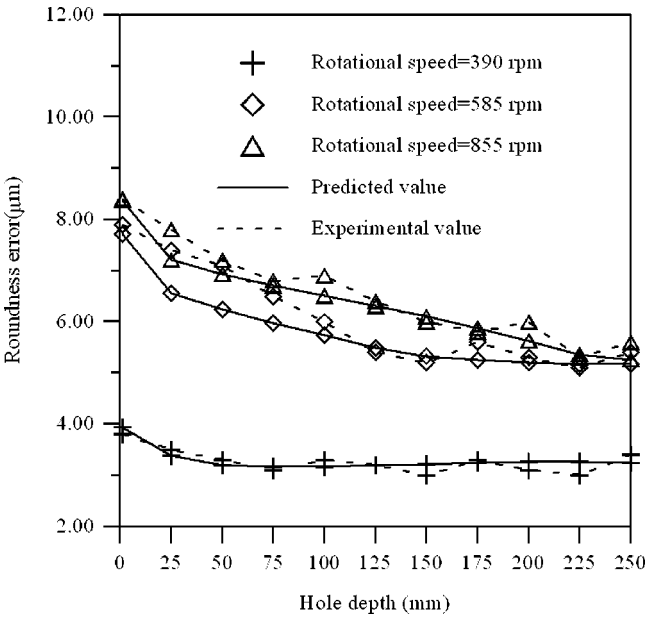


**Fig. 8 Influence of rotational speeds on the hole roundness error, tool diameter: 18.91 mm; feed rate: 0.1 mm/rev; shaft length: 1600 mm**

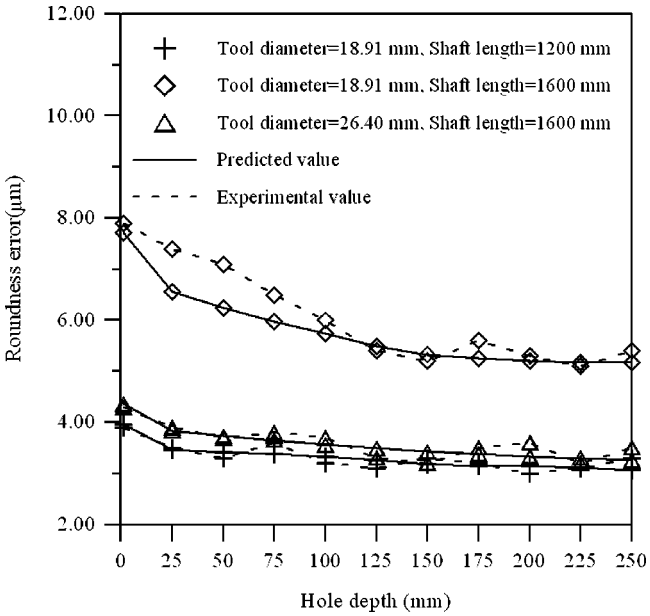


**Fig. 9 Influence of shaft lengths and tool diameters on the hole roundness error, rotational speed: 585 rpm; feed rate: 0.1 mm/rev**

Ramakrishna Rao [1] proposed an empirical equation containing cutting speed ($V_c$ m/min) and feed ($s$ mm/rev), as follows:

$$\text{Roundness error } (\mu\text{m}) = 9.3134 + 0.055V_c + 0.000944V_c^2 - 235.7s + 1587.3s^2$$

A comparison of theoretical values between Eq. (28) (calculated according to Eq. (29)) and Ramakrishna Rao's results is listed in Table 3. Again, the Eq. (28) stands in good agreement with the empirical equation from Ramakrishna Rao.

## 5 The Formation of the Multi-Corners

In deep-hole drilling the multi-corner hole is a bizarre phenomenon. Sakuma et al. [7,8] found in experiments that the multi-corner hole was generated by the chatter vibration of the machining system, which takes place at frequencies $f_c = n_c N/60$. They could propose an empirical equation for the number of hole corners:

$$n_c = \frac{60 f_c}{N} = kz_c \pm 1 \tag{38}$$

where $k$ is an integer and $z_c$ is the number of cutting edges (for BTA deep hole drill they took $z_c = 4$).

**Table 3 The mean roundness error as predicted by Eq. (28) and by Ramakrishna Rao [1], tool diameter: 20 mm; shaft length: 1600 mm**

| Feed rate (mm/rev) | Used equation | Mean roundness error ($\mu$m) | | |
|---|---|---|---|---|
| | | 390 rpm | 585 rpm | 855 rpm |
| 0.07 | Eq. (28) | 2.45 | 4.32 | 5.50 |
| | Ramakrishna Rao [1] | 2.51 | 3.89 | 6.27 |
| 0.10 | Eq. (28) | 3.51 | 5.81 | 7.44 |
| | Ramakrishna Rao [1] | 3.53 | 4.91 | 7.29 |

Ramakrishna Rao's empirical equation: [1] Roundness error ($\mu$m) = $9.3134 + 0.055V_c + 0.000944V_c^2 - 235.7s + 1587.3s^2$ where $V_c$ is the cutting speed in m/min and $s$ is the feed rate in mm/rev.

Gessesse et al. [9] found the following empirical relations while studying helical multi-lobe holes in BTA drilling: $n_c = 60 f_n / N$.

Multi-corner phenomenon was also observed in other hole-making processes. Bayly et al. [20] used a quasi-static model to analyze tool oscillation in reaming which issued following nondimensionalized tool whirling frequency (cyc/rev):

$$\text{Backward whirling} \quad \varpi_i^r \approx kz_c + 1, \quad k = 0,1,2,\ldots \tag{39a}$$

$$\text{Forward whirling} \quad \varpi_i^r \approx kz_c - 1, \quad k = 1,2,\ldots . \tag{39b}$$

In their case $z_c$ is the number of teeth on reamer and $\varpi_i^r$ corresponds to the number of lobes. Bayly et al.'s [20] number of lobes for reaming is equal to Sakuma et al.'s number of corners, Eq. (38), for deep-hole drilling. The whirling phenomenon for twist drill was experimentally observed and studied in [22,23], but no formula for number of corners was proposed.

Surprisingly, what Sakuma et al. [7,8] and Gessesse et al. [9] found for deep hole drilling, and Bayly et al. [20] (indirectly) found for reaming coincide with the theory given by Tlusty [19] for cutting waves on workpiece:

$$p + (\varepsilon/360) = f_c / Nz_c \tag{40}$$

If there is no phase shift $\varepsilon$, the number of waviness $p$ is practically the number of hole corners found by Sakuma et al. [7,8] or the number of lobes found by Gessesse et al. [9], or the number of lobes found by Bayly et al. [20]. Is the bizarre phenomenon "multi-corner" or "lobes" produced by deep hole drilling merely a pronounced phenomenon of cutting waves (undulations) on the hole wall?

Equation (28) enables an investigation into the variation of dynamic radial deflection on hole wall during the first four cycles of tool revolution at different shaft speeds, the results of which are shown in Figs. 10(a)(b)(c) for a tool shaft length of 1600 mm and tool diameter of 18.91 mm. In Fig. 10(a) the first cycle of cut (at 390 rpm) makes three complete waves and a residual phase of 0.8737 (81.21°). In Fig. 10(b), when at 585 rpm, there are two complete waves and a residual phase of 0.5826 (81.21°), and in Fig. 10(c), when at 855 rpm, there is only one wave and a residual phase of 0.7670 (156.26°). Equation (28) gives the following relationships correlating the number of waves, the residual phase, the tool natural frequency and the tool speed:

$$p + u = \frac{N_1}{N} \tag{41}$$

where $N_1$ is the first natural frequency calculated by $N_n = (30/\pi) \times (k_n \ell/\ell)^2 \times (\sqrt{EI/\rho A})$ [30] and listed in Table 4 ($k_n \ell$ is the value of the $n$th mode shown in Table 1). Equation (41) is exactly the same as that given by Tlusty [19], except in Eq. (41) it is the first tool natural frequency $N_1$ while in [19] it is the chatter frequency $f_c$. This speaks for a fact that the mechanism of hole lobes and workpiece waviness are the same. They are created either by chatter vibration or by resonant vibration.

In Eq. (40) Tlusty [19] used a chatter frequency approximately equal to one of the natural frequencies, but whether it is chatter frequency or natural frequency depends on the mechanisms actually involved.

One basic difference between Eq. (22) and the Tlusty's system [19] is that Eq. (22) does not include the regenerative effect. This means the multi-corners thus generated are of resonant nature, not regenerative nature. A thorough study of chatter frequencies by Insperger et al. [31] lead to identification of four different types of chatter frequencies in milling process: Chatters of self-excited nature have frequencies $f_H$ (due to the secondary Hopf bifurcation), $f_{PD}$ (due to the Period Doubling bifurcation) and chatters of resonant nature have frequencies $f_{TPE}$ (due to the Tooth Pass Excitation effect), $f_D$ (due to damped natural frequency). Many people,

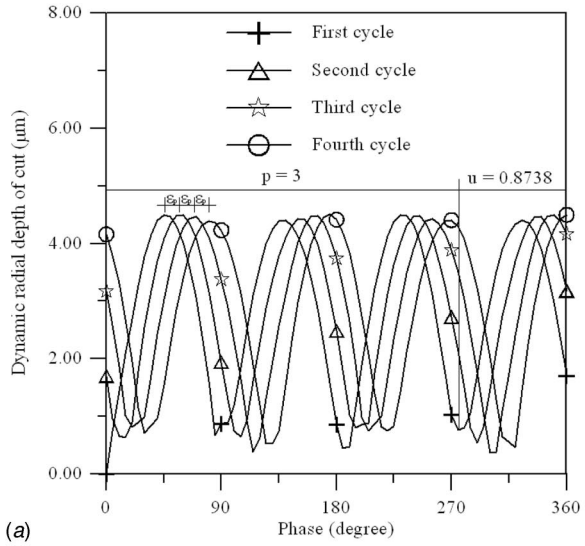


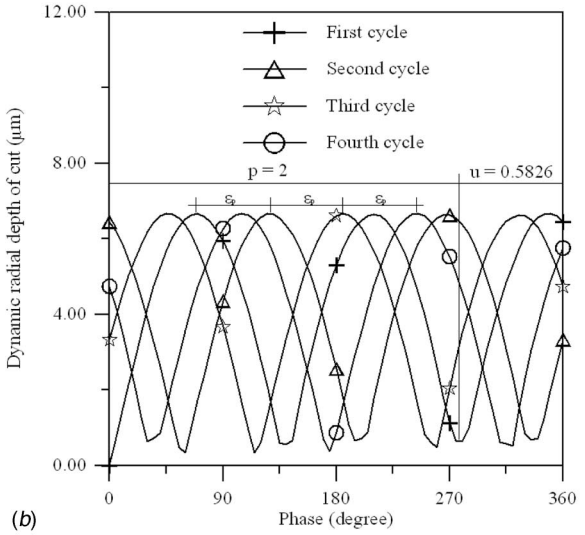


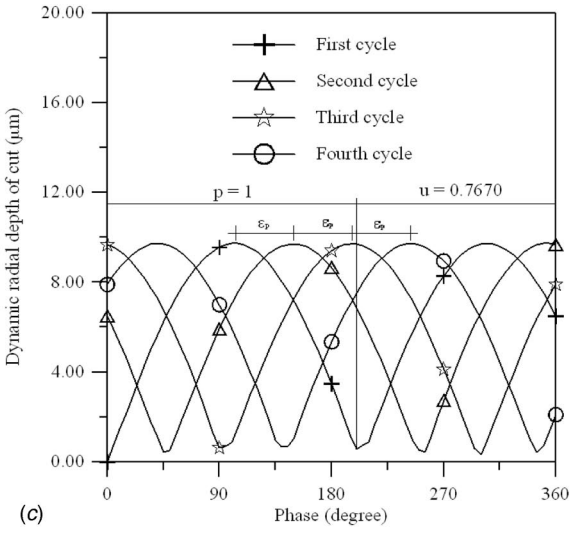


**Fig. 10 Influence of various rotational speeds on the wave phase, tool diameter: 18.91 mm; shaft length: 1600 mm; feed rate: 0.10 mm/rev. (a) Rotational speed: 390 rpm. (b) Rotational speed: 585 rpm. (c) Rotational speed: 855 rpm.**

**Table 4 The natural frequencies $N_n$ of the BTA tool shaft in mode $n=1\sim4$ with various tool diameters and shaft lengths. (Formula from [30]).**

| Tool diameter (mm) | Shaft length (mm) | $N_1$ (rpm) | $N_2$ (rpm) | $N_3$ (rpm) | $N_4$ (rpm) |
|---|---|---|---|---|---|
| 18.91 | 1200 | 2685.8 | 8703.8 | 18159.9 | 31054.4 |
| | 1600 | 1510.8 | 4895.9 | 10214.9 | 17468.1 |
| 26.40 | 1200 | 3412.4 | 11058.5 | 23072.7 | 39455.8 |
| | 1600 | 1919.5 | 6220.4 | 12978.4 | 22193.9 |

like Bayly et al. [21] didn't call $f_{TPE}$ chatter frequency but rather tooth-passing frequency which is low and associated with lobed holes.

The tooth-passing effect induced frequency $f_{TPE}$ are featured by [31]

$$f_{TPE}=\frac{kz_c\Omega}{60} \quad \text{where } \Omega \text{ is the tool speed.}$$

This is the same as that found by Sakuma et al. and Gessesse et al.

If the tool speeds become exactly an integer fraction of its natural frequency, say, if $N=N_1/2$, $N_1/3$, $N_1/4$, $N_1/5$ . . . etc., there is no residual phase but integer number of waves. The variations of dynamic radial deflection can be calculated by Eq. (28) and plotted in Figs. 11(a), (b), (c) and (d), in which all four cycles of tool rotation coincide exactly. There is no phase difference between consecutive cuttings hence the waves are in whole form. Figure 11(a)(b)(c)(d) show two, three, four and five waves on hole periphery produced by tool at speeds $N_1/2$, $N_1/3$, $N_1/4$, $N_1/5$ respectively.

After mapping the dynamic radial deflections of Figs. 11(a)(b)(c)(d) onto the profile of hole, the mysterious lobes of drilled hole appear, as can be seen in Figs. 12(a)(b)(c)(d), which show a hole of two, three, four and five lobes produced at tool speeds $N_1/2$, $N_1/3$, $N_1/4$ and $N_1/5$ respectively.

It is clear that the lobes, or multi-corners, are produced when the tool speed coincide with an integer fraction of its fundamental natural frequency. This explained the low-frequency feature observed for multi-cornered hole.

## 6 Conclusions

Hole distortion and lobes are long time problems in drilling. This work proposed a governing equation describing the drilling with pronounced shaft dynamics. The equation comprises Euler-Bernoulli beam equation representing the tool shaft and a radial excitation force, which took the form of Fourier series and was calibrated by an empirical cutting force equation. The solution of the proposed equation is the dynamic lateral deflection of the tool shaft, which turned out to give valuable knowledge about lobe mechanism.

Investigation reveals that the first mode ($n=1$) and the limited number of harmonics (e.g. $m=14$) dominate the contributions to the dynamic radial deflection. The dynamic radial deflection as given by Eq. (28) stands in good agreement with the empirical results from Ramakrishna Rao. Comparison between theoretical and experimental results regarding the influence of feed rates, tool speeds, tool diameters, tool shaft lengths on the hole roundness error proved the validity of the proposed equation.

The multi-corner (lobe) formation can be explained by solution of the proposed equation. A simulation using Eq. (28) gives a relation correlating the number of lobes, the residual phase, first natural frequency and the tool speed, which is exactly the same as the equation proposed by Tlusty for the dynamic waviness in milling generated by chatter. It is thus proven that the multi-corners (lobes) in drilling are in reality waviness generated by low-frequency vibration.

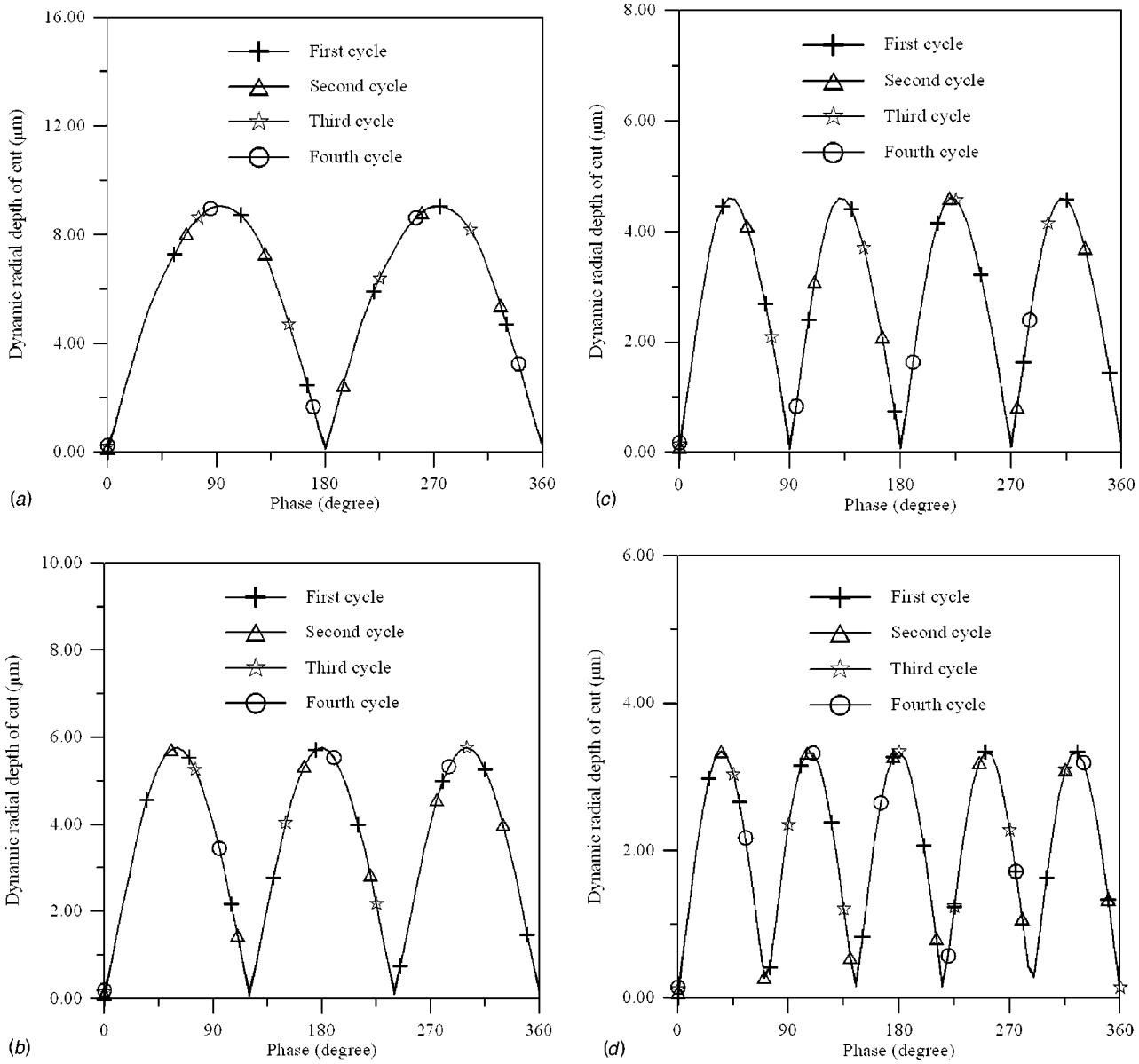


**Fig. 11 Influence of rotational speeds on the wave phase, tool diameter: 18.91 mm; shaft length: 1600 mm; feed rate: 0.10 mm/rev. (a) Rotational speed: $N_1/2=755.4$ rpm. (b) Rotational speed: $N_1/3=503.6$ rpm. (c) Rotational speed: $N_1/4=377.7$ rpm. (d) Rotational speed: $N_1/5=302.2$ rpm.**

The proposed equation differs from the analysis using typical mass-damping-stiffness model in that physical parameters including Young's modulus $E$, area moment of inertia $I$, cross-sectional area $A$, tool diameter $d$, rotational speed $N$, feed rate $s$, material density $\rho$, hole depth z, and tool length $\ell$ were explicitly addressed. Since the force model can be constructed and calibrated according to different real cutting force configurations, the proposed governing equation is useful for machining process in which the tool has significant shaft dynamics.

## Acknowledgment

The authors thank the anonymous reviewers for bringing two important works [20,31] to their attention.

## Nomenclature

$A$ = cross-sectional area of the tool shaft, $mm^2$
$E$ = Young's modulus of tool shaft, GPa
$I$ = cross-sectional area moment of inertia of tool shaft, $mm^4$
$N$ = rotational speed of the tool, rpm
$N_1$ = first natural frequency, rpm
$R$ = radius of the tool, mm
$\Delta R$ = dynamic radial deflection, $\mu$m
$c_w$ = speed of wave in the workpiece, m/sec
$d$ = tool diameter, mm
$f$ = radial excitation force, $kg\cdot m/sec^2$
$f_{Ax}$, $f_{Ay}$ = primary radial and tangential force component at A, $kg\cdot m/sec^2$
$f_{By}$, $f_{Cx}$ = radial force components of the burnishing pads B and C, $kg\cdot m/sec^2$
$f_{Bx}$, $f_{Cy}$ = tangential force components of the burnishing pads B and C, $kg\cdot m/sec^2$
$f_{tx}$, $f_{ty}$ = drill head forces in x-, y-direction, $kg\cdot m/sec^2$
$f_{dx}$, $f_{dy}$ = cutting forces in x-, y-direction, $kg\cdot m/sec^2$
$f_c$ = chatter frequency of the machining system, Hz

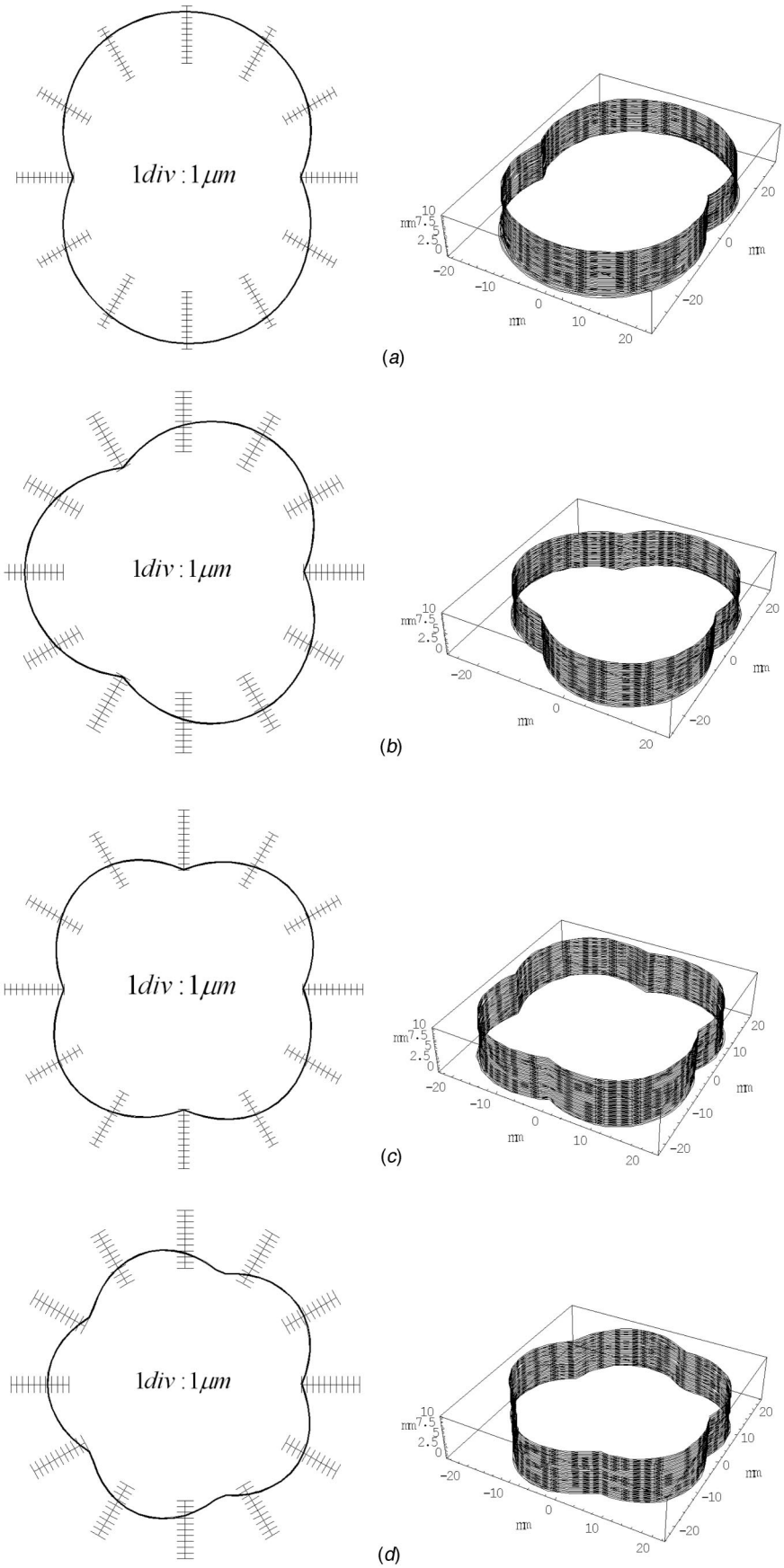


**Fig. 12 Influence of various rotational speeds on the hole profile, tool diameter: 18.91 mm; shaft length: 1600 mm; feed rate: 0.1 mm/rev; hole depth: 1 mm. (a) Rotational speed: $N_1/2=755.4$ rpm. (b) Rotational speed: $N_1/3=503.6$ rpm. (c) Rotational speed: $N_1/4=377.7$ rpm. (d) Rotational speed: $N_1/5=302.2$ rpm.**

$f_n$ = lateral natural frequency of the machining system, Hz
$k_n$ = undetermined constants of $n$th modes
$\ell$ = tool shaft length, mm
$n_c$ = the corner (lobe) number of hole profiles.
$p$ = number of waviness on workpiece profile
$s$ = feed rate, mm/rev
$u$ = phase of the residual wave
$\Delta x$, $\Delta y$ = cutting depth in the x and y directions, respectively.
$z$ = hole depth
$z_c$ = number of teeth of the cutter
$\alpha_B$, $\alpha_C$ = angles of the burnishing pads B and C from cutting edge, respectively, degree
$\varepsilon$ = phase shift
$\varepsilon_p$ = phase error of two cycles waves, degree
$\omega$ = the angular speed of the tool, $\omega = \pi N/30$ (rad/sec)
$\theta$ = the rotational angle of the tool, $\theta = \omega t$
$\rho$ = mass density of tool shaft, kg/m$^3$

## Appendix A

$$q_{10} = EIk_n^4 + \rho A(A - \omega^2)$$

$$q_{11}(t) = e^{jt(EIk_n^4/\rho A\omega^2)/2\omega}$$

$$q_{12}(t) = \frac{At}{2\omega}$$

$$q_{13}(t) = \{1 - q_{11}(t)[\cos(q_{12}(t)) + j\sin(q_{12}(t))]\}/q_{10}$$

$$\begin{aligned} q_{14}(t)|_\alpha = \{&[\cos(m\alpha) - j\sin(m\alpha)]/q_{10} - \{2q_{11}(t)[(q_{10} \\ &- 2m\rho A\omega^2)\cos(m\alpha) + 2jm\rho A\omega^2 \sin(m\alpha)] \\ &\times [\cos(q_{12}(t)) + j\sin(q_{12}(t))]\}/[q_{11}(t)(q_{11}(t) \\ &- 4m\rho A\omega^2)] + [\cos(m\alpha + 2mt\omega) + j\sin(m\alpha \\ &+ 2mt\omega)]/(q_{11}(t) - 4m\rho A\omega^2)\}/2 \end{aligned}$$

$$\begin{aligned} q_{15}(t)|_\alpha = \{&[j\cos(m\alpha) + \sin(m\alpha)]/q_{10} - \{2q_{11}(t)[(q_{10} \\ &- 2m\rho A\omega^2)\sin(m\alpha) - 2jm\rho A\omega^2 \cos(m\alpha)] \\ &\times [\cos(q_{12}(t)) + j\sin(q_{12}(t))]\}/[q_{11}(t)(q_{11}(t) \\ &- 4m\rho A\omega^2)] + [\sin(m\alpha + 2mt\omega) - j\cos(m\alpha \\ &+ 2mt\omega)]/(q_{11}(t) - 4m\rho A\omega^2)\}/2 \end{aligned}$$

$$\begin{aligned} q_6(t) = (a_{0A} + a_{0B} + a_{0C})q_{13}(t)/2 + \sum_{m=1}^{\infty} \{&[a_{mA}q_{14}(t)|_{\alpha=0} \\ &+ a_{mB}q_{14}(t)|_{\alpha=\alpha_B} + a_{mC}q_{14}(t)|_{\alpha=\alpha_C}]e^{-jm\omega\ell/c_w} \end{aligned}$$

$$\begin{aligned} q_7(t) = \sum_{m=1}^{\infty} \{&[b_{mA}q_{15}(t)|_{\alpha=0} + b_{mB}q_{15}(t)|_{\alpha=\alpha_B} \\ &+ b_{mC}q_{15}(t)|_{\alpha=\alpha_C}]e^{-jm\omega\ell/c_w}\} \end{aligned}$$

## Appendix B

Experimental equipment:
1. Lathe San Shing SK26120 Heavy Duty Precision Lathe
BTA drilling system (Fig. 3)
2. BTA drilling
(a) Tool head: SANDVIK 420.6 series
(b) Tool shaft: Type: SANDVIK 420.5-800-2
• Tool head: 18.91 and 19.90 mm, internal and external diameters of tool shaft: 11.5 and 17 mm, respectively
• Tool head: 24.11 and 26.40 mm, internal and external diameters of tool shaft: 14 and 22 mm, respectively
Material: JIS SNCM 21 Density $\rho$: 7860 kg/m$^3$
Young's modulus $E$: $206 \times 10^9$ Pa
3. Cutting Fluid: Type: R32; Density $\rho_f$: 871 kg/m$^3$
Absolute viscosity $\mu$: 0.383 kg/m·sec
4. Dynamometer: Model: 6423-3K S/N 140 from Lebow
Rated capacity (compression only): 1360.8 kg (3000 lb)
Max. load (without zero shift): 50% overload (150% of rated capacity)
Signal sensors: 4 arm bonded strain gauge bridges

## References


[1] Ramakrishna Rao, P. K., and Shunmugam, M. S., 1987, "Accuracy and Surface Finish in BTA," Sov. Powder Metall. Met. Ceram, **25**(1), pp. 31–44.
[2] Ramakrishna Rao, P. K., and Shunmugam, M. S., 1987, "Investigation: Stress in Boring Trepanning Association Machining," Wear, **119**, pp. 89–100.
[3] Ramakrishna Rao, P. K., and Shunmugam, M. S., 1987, "Analysis of Axial and Transverse Profiles of Holes Obtained in B.T.A. Machining," Int. J. Mach. Tools Manuf., **27**(4), pp. 505–515.
[4] Ramakrishna Rao, P. K., and Shunmugam, M. S., 1988, "Wear Studies in Boring Trepanning Association Drilling," Wear, **124**, pp. 33–43.
[5] EI-Khabeery, M. M., Saleh, M. M., and Ramadan, M. R., 1991, "Some Observations of Surface Integrity of Deep Drilling Holes," Wear, **142**, pp. 331–349.
[6] Sakuma, K., Taguchi, K., and Katsuki, A., 1980, "Study on Deep-Hole-Drilling With Solid-Boring Tool—the Burnishing Action of Guide Pads—and Their Influence on Hole Accuracies," Bulletin of the Japan Society of Mechanical Engineering , **23**, pp. 1921–1928.
[7] Sakuma, K., Taguchi, K., and Katsuki, A., 1980, "Study on Deep-Hole Boring by BTA System Solid Boring Tool—Behavior of Tool and Its Effects on Profile of Machined Hole," Bull. Jpn. Soc. Precis. Eng., **14**(3), pp. 143–148.
[8] Sakuma, K., Taguchi, K., and Katsuki, A., 1981, "Self-Guiding Action of Deep-Hole-Drilling Tools," CIRP Ann., **30**, pp. 311–315.
[9] Gessesse, Y. B., Latinovic, V. N., and Osman, M. O. M., 1994, "On the Problem of Spiralling in BTA Deep-Hole Machining," ASME J. Eng. Ind., **116**, pp. 161–165.
[10] Chin, J. H., and Lin, S. A., 1996, "Dynamic Modelling and Analysis of Deep Hole Drilling Process," Int. J. Model. Simulat., **16**(3), pp. 157–165.
[11] Chandrashekhar, S., Sankar, T. S., and Osman, M. O. M., 1987, "A Stochastic Characterization of the Machine Tool Workpiece System in BTA Deep Hole Machining—Part I. Mathematical Modelling and Analysis," Advanced Manufacturing Processes, **2**(1&2), pp. 37–69.
[12] Chandrashekhar, S., Sankar, T. S., and Osman, M. O. M., 1987, "A Stochastic Characterization of the Machine Tool Workpiece System in BTA Deep Hole Machining—Part II. Mathematical Modelling and Analysis," Advanced Manufacturing Processes, **2**(1&2), pp. 71–104.
[13] Chin, J. H., Wu, J. S., and Young, R. S., 1993, "The Computer Simulation and Experimental Analysis of Chip Monitoring for Deep Hole Drilling," ASME J. Eng. Ind., **115**, pp. 184–192.
[14] Chin, J. H., and Wu, J. S., 1993, "Mathematical Models and Experiments for Chip Signals of Single-Edge Deep Hole Drilling," Int. J. Mach. Tools Manuf., **33**(3), pp. 507–519.
[15] Deng, C. S., Huang, J. C., and Chin, J. H., 2001, "Effects of Support Misalignments in Deep-Hole Drill Shafts on Hole Straightness," Int. J. Mach. Tools Manuf., **41**(8), pp. 1165–1188.
[16] Chin, J. H., and Lee, L. W., 1995, "A Study on the Eigenproperties of BTA Deep-Hole Drill—Theory and Experiments," Int. J. Mach. Tools Manuf., **35**(1), pp. 29–49.
[17] Chin, J. H., and Hsieh, C. T., 1996, "The Shaft Behavior of BTA Deep Hole Drilling Tool," Int. J. Mech. Sci., **38**(5), pp. 461–482.
[18] Perng, Y. L., and Chin, J. H., 1999, "Theoretical and Experimental Investigations on the Spinning BTA Deep-Hole Tool Shafts Containing Fluids and Subject to Axial Forces," Int. J. Mech. Sci., **41**, pp. 1301–1322.
[19] Tlusty, J., 1986, "Dynamics of High-Speed Milling," ASME J. Eng. Ind., **108**, pp. 59–67.
[20] Bayly, P. V., Young, K. A., Calvert, S. G., and Halley, J. E., 2001, "Analysis of Tool Oscillation and Hole Roundness Error in a Quasi-Static Model of Reaming," ASME J. Manuf. Sci. Eng., **123**, pp. 387–396.
[21] Bayly, P. V., Lamar, M. T., and Calvert, S. G., 2002, "Low-Frequency Regenerative Vibration and the Formation of Lobed Holes in Drilling," ASME J. Manuf. Sci. Eng., **124**, pp. 275–285.
[22] Fujii, H., Marui, E., and Ema, S., 1986, "Whirling Vibration in Drilling. Part 1: Cause of Vibration and Role of Chisel Edge," ASME J. Eng. Ind., **108**, pp. 157–162.
[23] Ema, S., Fujii, H., and Marui, E., 1988, "Whirling Vibration in Drilling. Part 3: Vibration Analysis in Drilling Workpiece With a Pilot Hole," ASME J. Ind., **110**, pp. 315–321.
[24] Griffiths, B. J., 1993, "Modeling Complex Force Systems—Part 1: The Cutting and Pad Forces in Deep Drilling," ASME J. Eng. Ind., **115**, pp. 169–176.
[25] Matin, M. A., and Rahman, M., 1988, "Analysis of the Cutting Process of a Cylindrical Workpiece Clamped by a Three-Jaw Chuck," ASME J. Eng. Ind., **110**, pp. 326–332.
[26] Rahman, M., Matin, M. A., and Seah, K. H. W., 1993, "A Study of the

Vibrational Dynamics of an Endrill Clamped by Side-Locking,'' ASME J. Eng. Ind., **115**, pp. 438–443.
[27] Kreyszig, E., 1993, *Advanced Engineering Mathematics* (7th Edition), p. 287, John Wiley & Sons, Inc.
[28] Shunmugam, M. S., 1991, ''Criteria for Computer-Aided Form Evaluation,'' ASME J. Ind., **113**, pp. 233–238.
[29] Chandrashekhar, S., Osman, M. O. M., and Sankar, T. S., 1984, ''An Analytical Time Domain Evaluation of the Cutting Forces in BTA Deep Hole Machining Using the Thin Shear Plane Model,'' Sov. Powder Metall. Met. Ceram, **22**, pp. 697–721.
[30] Dimarogonas, A., 1996, *Vibration for Engineering* (Second Edition), Prentice Hall International Editions, New Jersey, Chapters 4 and 9.
[31] Insperger, T., Stepan, G., Bayly, P. V., and Mann, B. P., 2003, ''Multiple Chatter Frequencies in Milling Processes,'' J. Sound Vib., **262**, pp. 333–345.